Sensors and Actuators B 227 (2016) 419–426

Contents lists available at ScienceDirect

Sensors and Actuators B: Chemical

journal homepage: www.elsevier.com/locate/snb

Improvement of NO_2 gas sensing performance based on discoid tin oxide modified by reduced graphene oxide

Yan Xiao, Qiuyue Yang, Zhenyu Wang, Rui Zhang, Yuan Gao*, Peng Sun, Yanfeng Sun, Geyu Lu*

State Key Laboratory on Integrated Optoelectronics, College of Electronic Science and Engineering, Jilin University, 2699 Qianjin Street, Changchun 130012, China

ARTICLE INFO

Article history:
Received 5 June 2015
Received in revised form 9 November 2015
Accepted 12 November 2015
Available online 17 December 2015

Keywords:
Tin oxide
Graphene
Gas sensor
Metal oxide semiconductor

ABSTRACT

A facile one-step hydrothermal method for a novel discoid crystal of rutile SnO_2 modified by reduced graphene oxide (rGO) is reported in this work. X-ray powder diffraction (XRD), X-ray photoelectron spectroscopy (XPS), field emission scanning electron microscopy (FESEM) and transmission electron microscopy (TEM) were performed to characterize the structure and morphology of the SnO_2/rGO composites. Uniform discoid rutile SnO_2 monocrystal with a diameter of approximately 100 nm and a center thickness of 40 nm was anchored on both sides of rGO nanosheets. The SnO_2/rGO composite exhibited preferential detection toward NO_2 with high response, good selectivity and reproducibility. The response of the sensor to 1 ppm NO_2 at 75 °C was nearly one order of magnitude higher than that of SnO_2, and the detection limit was improved to 50 ppb. The improved response was discussed and the gas sensing mechanism was established.

1. Introduction

Since air pollution has become an urgent global problem with the development of industry and technology, detecting gases, especially toxic gases as the basis for controlling air pollution, has become increasingly significant. NO_2 is a toxic compound produced by combustion in power plants and combustion engines. This gas is harmful to the environment and is a major cause of acid rain, photochemical smog and pollution haze. EPA recently established a new 1-h standard at 0.1 ppm, which is well below the values fixed by previous safety guidelines, to provide requisite protection of public health [1–3].

Among the different types of gas sensors, metal oxides (MOS) semiconductor sensors are widely used in toxic and flammable gas detection because of their sensitivity, selectivity and stability. SnO_2 is an important n-type semiconductor with a wide band gap (E_g = 3.6 eV), which was first reported in the 1990s. It is one of the most intensively investigated materials because of its widely important applications such as gas sensors [4,5], solar cells [6,7], lithium-ion batteries [8,9] and transparent electronics [10]. Most high-response SnO_2 sensors typically operate at high temperatures of over 200 °C for enhanced adsorption and reactivity. However, high temperatures intensify the aggregation between particles, and high working temperatures lead to power waste. Existing SnO_2 sensors with low operating temperatures usually show poor gas sensing performance, especially in detection limit, response and recovery time. Given the fact that the composition, size and morphology of MOS exhibit a considerable impact on their properties, tremendous efforts have been devoted to improving the performance of MOS semiconductor sensors. The formation of a heterojunction by introducing other promising materials into composites also enhances the sensing performance. Numerous studies have proved that the p–n heterojunction formed by n-type and p-type materials can play a positive role in the sensing process [11–15].

Graphene is a single-layer sp^2 carbon atom lattice. This material, has become a star compound for gas sensors because of its outstanding qualities, such as high charge carrier mobility, mechanical robustness, large surface area (2630 $m^2 g^{-1}$) [16], special optical propertieies, and good thermal stability. Graphene and reduced graphene oxide (rGO)-based nanostructures have been widely studied for gas sensor applications because of their high sensitivity to electrical perturbations from gas molecule adsorption as a result of their ultra-small thickness [17]. rGO has lower conductivity, more dangling bonds and defect than intrinsic graphene, which do good to its adsorption and interaction with target gas.

* Corresponding authors. Tel.: +86 43185167808; fax: +86 43185167808.
E-mail addresses: gaoyuan@jlu.edu.cn (Y. Gao), lugy@jlu.edu.cn (G. Lu).

http://dx.doi.org/10.1016/j.snb.2015.11.051
0925-4005/

Some research groups recently introduced graphene or rGO to MOS-based materials, and obtained unique structure composites to improve sensing performance. MOS/rGO was proved to be effective for constructing high-performance gas sensors [18–20]. Pinna reported a room-temperature hydrogen sensor based on SnO_2/rGO and Pt–SnO_2/rGO [21]. Highly aligned SnO_2 nanorods on graphene sheets were synthesized to enhance the sensitivity to H_2S at the operating temperature of 260 °C [22]. Selective acetone and hydrogen sulfide sensors based on SnO_2 nanofibers functionalized with rGO nanosheets were fabricated at operating temperatures of 200 °C and 350 °C, respectively [23]. The NH_3 sensing performance of flower-like SnO_2/rGO composites was investigated at room temperature [24]. Zhang et al. found that SnO_2 nanoparticles/rGO composites exhibited high response to NO_2 at low operating temperature (50 °C) [25]. And high-performance NO_2 sensing of 3D mesoporous rGO aerogel-supported SnO_2 nanocrystals was studied at low temperature [26]. Although the studies on SnO_2/rGO have improved the NO_2 sensing performance compared to intrinsic graphene at room temperature or relative low operating temperature, their gas sensing response and detection limit should still be developed further.

In this work, SnO_2/rGO with a novel structure was synthesized through a facile one-step hydrothermal method. The SnO_2 in the composites was discoid rutile monocrystalline with rough surface. The sensors based on the SnO_2/rGO composites were fabricated, and their NO_2 sensing performance was investigated. The SnO_2/rGO exhibited n-type semiconductor behavior in the gas sensing process because of the small amount of rGO. Investigations on gas sensors showed that sensors based on SnO_2/rGO composites exhibited more than one order of magnitude improvement in the response and a shorter response time compared with that of individual SnO_2.

2. Experimental

2.1. Materials

All chemicals were the analytical-grade reagents and used without any other further purification. Graphite powder, potassium peroxydisulfate, phosphorus pentoxide, potassium permanganate, sulfuric acid, sodium citrate ($Na_3C_6H_5O_7{\bullet}2H_2O$), stannous sulfate were purchased from Sinopharm Chemical Reagent Co. Ltd. (China).

2.2. Instrumentation

X-ray diffraction (XRD) patterns of the as-prepared products were conducted on a Rigaku D/max-2500 X-ray diffractometer using Cu-Ka radiation, at a scanning speed of 12°/min. Field emission scanning electron microscope (SEM) was taken on a JEOL JSM-7500F microscope operating at 15 kV. Transmission electron microscopy (TEM), high resolution transmission electron microscopy (HRTEM), and selected-area electron diffraction (SAED) were conducted on a JEOL JEM-3010 microscope with an accelerating voltage of 200 kV. X-ray photoelectron spectroscopy (XPS) was conducted on an ESCALAB MKII X-ray photoelectron spectrometer.

2.3. Synthesis and characterization of the SnO_2/rGO composite

Graphene oxide (GO) was prepared by a modified Hummer's method as described in reference [27]. The SnO_2/rGO material was synthesized via a hydrothermal method with $SnSO_4$ and GO as precursors. In a typical process, 0.1 g $SnSO_4$ and 1.37 g $Na_3C_6H_5O_7{\bullet}2H_2O$ were dissolved in 32 mL mixture of deionized water and glycerol (5:3, v:v) under continuous stirring. Then 1.37 mL HCl (38%) was added into the above solution and following with aliquot GO solution (0.5 mg, 1 mg, 2 mg). After 30 min vigorous stirring, the mixture which had formed a homogeneous solution was transferred into a Teflon-lined stainless-steel autoclave and maintained at 180 °C for 24 h. After the hydrothermal procedure, the autoclave cooled down naturally to room temperature. Afterward, the product was collected by centrifugation and washed several times with deionized water, and dried at −50 °C. Finally, a series of SnO_2/rGO composites with 0.7, 1.4 and 2.8 wt.% rGO was obtained. For control experiments, rGO and pure SnO_2 were prepared under the same condition with only GO and without adding GO respectively. All samples were freeze-dried without any treatment before characterization.

2.4. Fabrication and measurement of gas sensors

The gas sensors were fabricated as follows: the as-prepared materials were mixed with deionized water to form slurry, and made a uniform thick coating layer using a small brush with the slurry onto an alumina tube (4 mm in length, 1.2 mm in external diameter, 0.8 mm in internal diameter) which was attached with a pair of gold electrodes. After the coating layer drying in air at room temperature, the alumina tube was heat treated at 350 °C for 2 h. In order to control the operating temperature of sensors, a Ni–Cr alloy coil was inserted to the alumina tube as a heater. The gas-sensing properties were investigated using a RQ-2 series Intelligent Test Meter (China) by testing the changing of resistances of the coating layer when the tube was exposed in air and tested gases atmosphere under laboratory conditions (30 RH%, 22 °C). The gas-sensing properties of the sensors were measured with a static gas-sensing characterization system, environmental air was used as both a reference gas and a diluting gas to obtain desired concentrations of target gases. A typical testing procedure was as follows. Firstly, the sensor was put into the chamber of air to get a steady state, then the sensor was took to another chamber filled with the uniform tested gas, which was injected with calculated amount. When the response reached a constant value, the sensor was transferred back to chamber containing air and kept there until complete recovery. The response of the gas sensor is defined as the ratio of the resistance of the sensor in the tested gases (R_g) to that in air (R_a). For oxidizing tested gases, that is Response = R_g/R_a, while for the reducing tested gases, Response = R_a/R_g. The response and recovery time is defined as the time taken by the sensor to achieve 90% of the total resistance change in the case of adsorption and desorption respectively.

3. Results and discussion

3.1. Morphological and structural characteristics

The XRD patterns of the crystallographic structure of GO, rGO, SnO_2 and SnO_2/rGO composites are shown in Fig. 1. The diffraction peak at around $2\theta = 11.2°$ in Fig. 1a belongs to the (0 0 1) reflection of GO. The rGO sample showed two characteristic diffraction peaks at 24.4° and 42.8°, which corresponded to the (0 0 2) and (1 0 0) planes of graphene, indicating that GO was reduced to rGO via the hydrothermal treatment [28]. All diffraction peaks in the SnO_2 patterns could be clearly indexed to rutile SnO_2 according to JCPDS card No. 41-1445. The mean spherical crystallite size of the SnO_2 calculated by the Scherrer equation was 53 nm. The pattern of SnO_2/rGO was similar to that of SnO_2, and no obvious diffraction peaks of rGO were observed owing to small amount of rGO in the composites and its intrinsic weak diffraction intensity.

The morphology and microstructure of the samples were characterized using field-emission scanning electron microscopy (FESEM). As shown in Fig. 2a, b, the GO exhibited the wrinkled flaky structure, and the obtained rGO after hydrothermal treatment showed a more curly structure and aggregation. SEM images of the SnO_2 and SnO_2/rGO are shown in Fig. 2c, d. The SnO_2 particles with

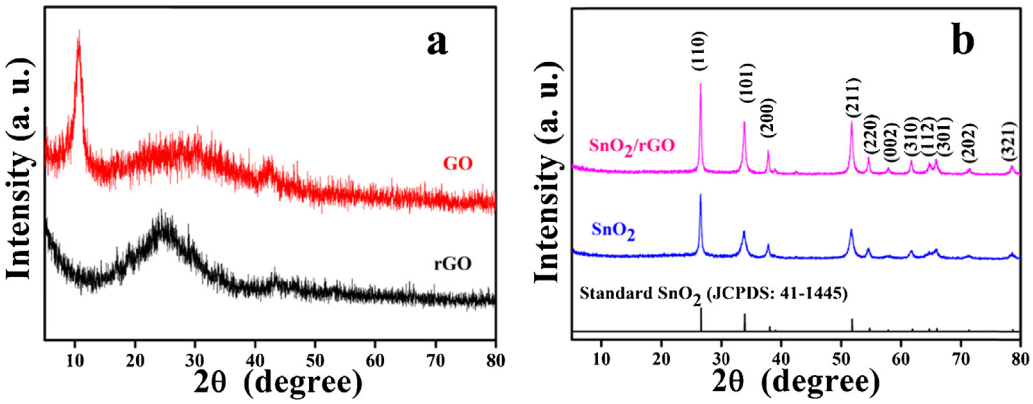

Fig. 1. XRD patterns of GO, rGO (a), SnO_2 and SnO_2/rGO (b).

relatively uniform size distribution were tightly stacked. For the sample of SnO_2/rGO, it can be observed that the SnO_2 particles are stacked on both sides of rGO sheets. Due to the low percentage of rGO, rGO sheets were wrapped by SnO_2 nanoparticles with few visible edges. In local magnification (Fig. 2e, f), the discoid SnO_2 with rough surface were shown from different lateral positions, as well as flaky rGO edges among the monodisperse SnO_2 discoid particles. The morphology and size of SnO_2 were approximately the same irrespective of the presence or absence of rGO, suggesting that loading of rGO did not noticeably affect the growth of SnO_2.

A detailed TEM was performed to further investigate the crystal structure of the SnO_2 discoid particles. Fig. 3a, b, showed the TEM image of individual SnO_2 nanoparticle. The morphology of SnO_2 is shown as discoid particles with rough surface which were in good accord with the FESEM observations. And the detail of a single "discus" revealed a clear and well-defined discoid structure

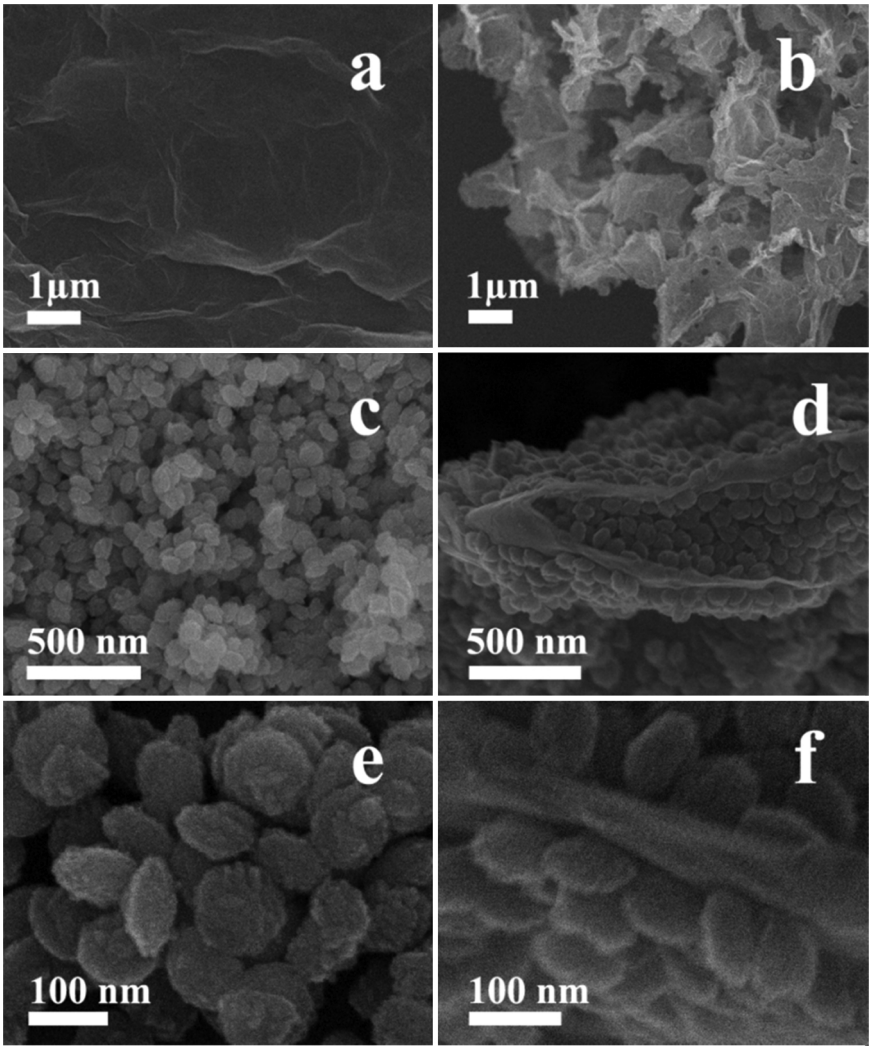

Fig. 2. FESEM images of GO (a), rGO (b), SnO_2 (c, e), SnO_2/rGO (d, f).

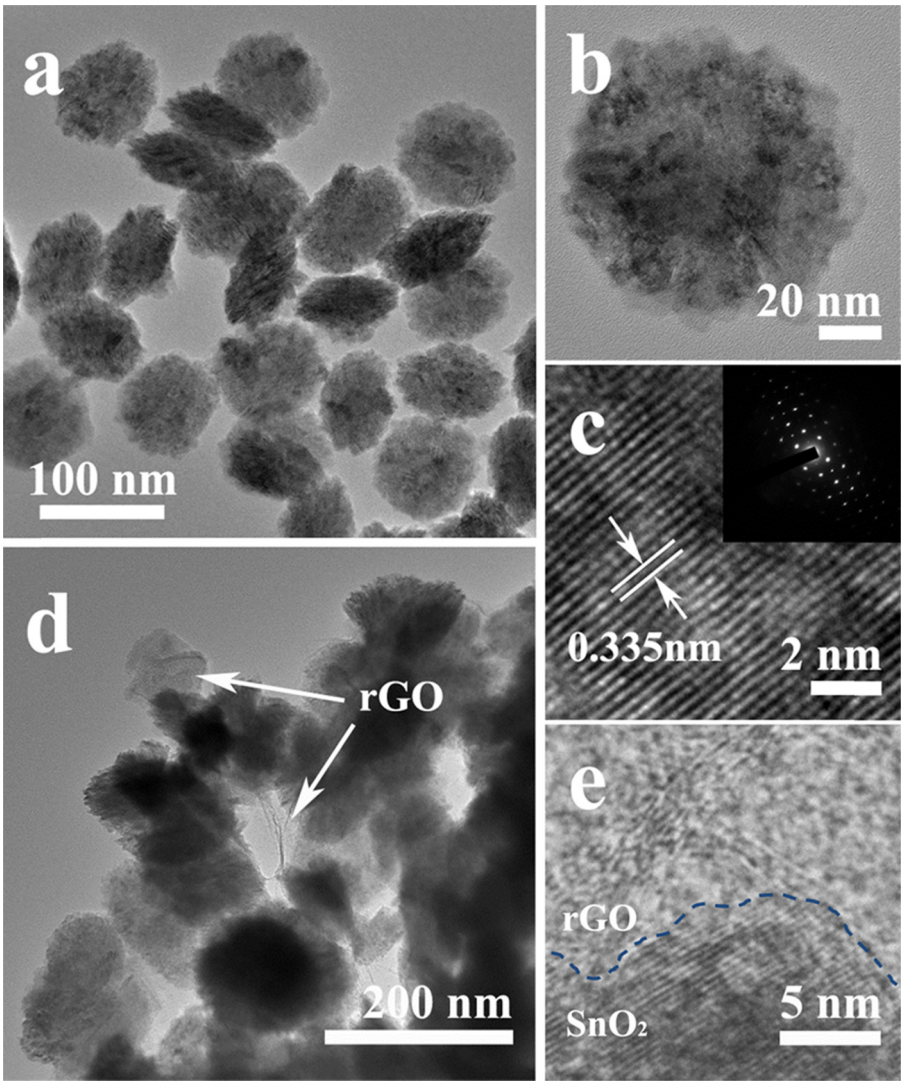

Fig. 3. Typical TEM images of SnO_2 nanoparticles (a, b) and SnO_2/rGO composites (d). HRTEM images of SnO_2 nanoparticles (c) and SnO_2/rGO composites (e). The inset in (c) is the corresponding SAED pattern.

with a diameter of approximatey 100 nm and a center thickness of about 40 nm. The HRTEM image (Fig. 3c) exhibits that the fringe distance is 0.335 nm which corresponds to the lattice distances of the (1 1 0) plane of rutile SnO_2 [29]. The SAED pattern of an individual "discus" (the inset in Fig. 3c shows the single crystalline nature). Fig. 3d illustrates the TEM image of the SnO_2/rGO composite, SnO_2 particles were compactly anchored on both sides of rGO sheets. The rGO sheets with clear wrinkles were obviously observed in the composites. In the HRTEM image, both the lattice of SnO_2 and rGO wrinkles can be observed at the junction of SnO_2/rGO composites (Fig. 3e).

The surface composition and element analysis for the as-prepared products were characterized by an XPS. As shown in Fig. 4a, the XPS spectra of GO and SnO_2/rGO both reveal two peaks at 284.6 and 532.2 eV, corresponding to C 1s and O 1s, respectively. The other two strong peaks at 486.1 eV and 494.5 eV were also observed on the spectrum of the composites, which were associated with Sn 3d. The high-resolution C1s XPS spectrum of

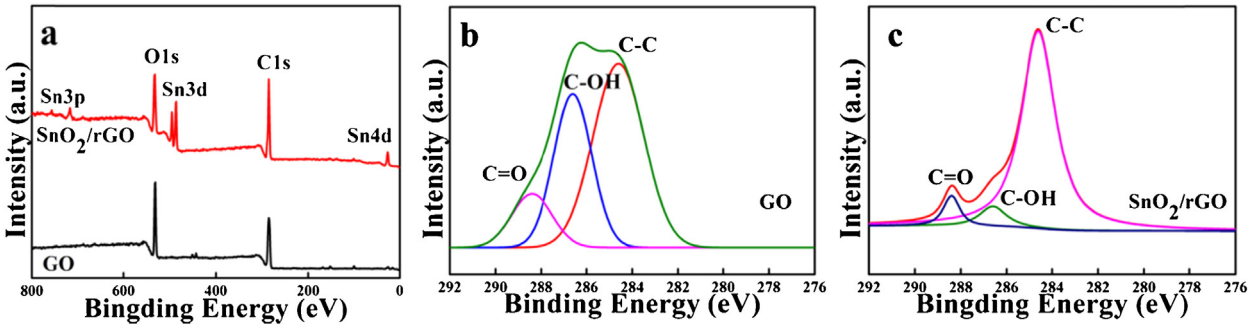

Fig. 4. XPS spectra of GO and SnO_2/rGO composite (a). C1s spectra of GO (a), and SnO_2/rGO composite (c).

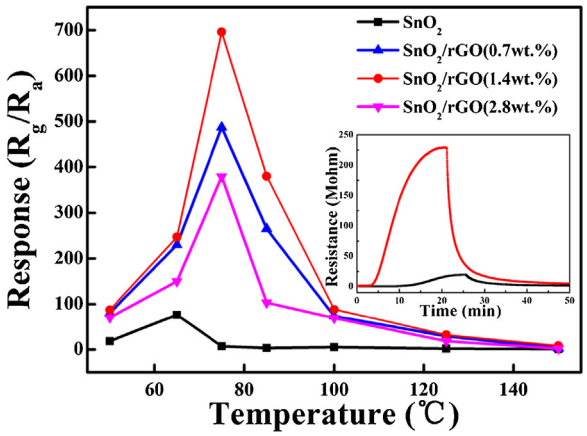

Fig. 5. Response of sensor based on SnO_2/rGO and SnO_2 to 1 ppm NO_2 as a function of the operating temperature. The inset is response transient curves of SnO_2/rGO and SnO_2 to 1 ppm NO_2 at 75 °C and 65 °C, respectively.

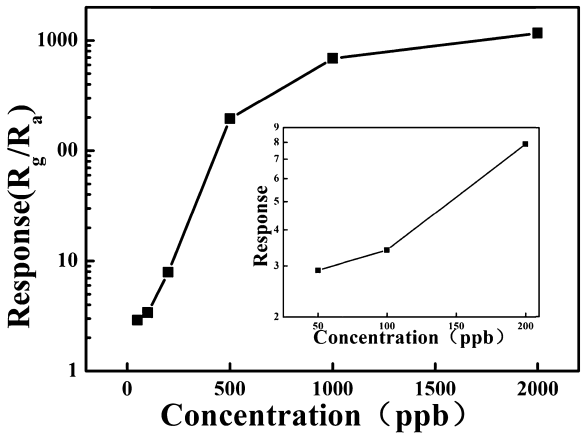

Fig. 6. The response of sensor based on SnO_2/rGO to different concentrations NO_2 at 75 °C.

GO and SnO_2/rGO (Fig. 4b, c) showed peaks at 284.6, 286.6 and 288.4 eV, accounting for the C–C, C–OH and C=O [30,31]. The intensities of C–O and C=O were much weaker in SnO_2/rGO than in GO. The results suggested that most oxygen containing groups were removed during the hydrothermal treatment. Thus, the GO was successfully reduced to rGO.

3.2. Gas-sensing properties to NO_2

In order to investigate the properties of the SnO_2/rGO composites, a series of gas-sensing tests were conducted and the results are shown as follows. The operating temperature is an important factor in the gas sensing properties of materials. In the Fig. 5, the response to 1 ppm NO_2 of the sensor based on SnO_2/rGO composites with different percentages of rGO as a function of the operating temperature. The responses of all the SnO_2/rGO composites at any tested temperature were higher than that of SnO_2, which indicated that the introduction of rGO can enhance response to NO_2 with varying degrees. Sensor response of SnO_2/rGO with 1.4 wt.% rGO reached a maximum value at 75 °C, which was enhanced by nearly 10 times that of pure SnO_2. However, an insufficient but additional content of rGO decreased the gas responses. When the percentage of rGO is insufficient, the resistance modulation of rGO is limited (discussed in mechanism section). When the percentage of rGO exceeds the critical rGO content, additional conducting channel will be formed and the percolation will happen in the composites, resulting in the decrease of the response. In this case, p-type rGO sheets will connect with neighboring rGO, promoting hole current flow through the continuous rGO layer, which acts as parallel resistance and reduces the total resistance. The response of the sensors based on SnO_2/rGO composites showed the highest value to NO_2 at 75 °C, and decreased when increasing the operating temperature above 75 °C. Gases react optically with chemisorbed oxygen on metal oxides semiconductor at a particular temperature, which makes the resistance in tested gases varying significantly [32]. There is not enough energy to make full reaction between oxygen species and NO_2 when the temperature is below 75 °C. At temperature of 75 °C, all the oxygen species may have the required energy to react with NO_2 molecules. But when the temperatures is above 75 °C, the amount of oxygen ion species adsorbed on the surface sites of the SnO_2 may be insufficient to react with NO_2 molecules, and more electrons will jump into the conduction band at higher temperatures, so the resistance in air (R_a) and the response ($R = R_a/R_g$) will decrease [33]. Therefore, further gas sensing studies based on SnO_2/rGO were conducted with the sample of 1.4 wt.% rGO at the optimum operating temperature of 75 °C.

The response and recovery time should be evaluated as important parameters of sensors. In the inset of Fig. 5, the transient response curves of the SnO_2/rGO and SnO_2 at respective optimum operating temperature were shown. It can be seen that not only the response value but also the response and recovery time were improved due to the presence of rGO in samples. The response and recovery time of the sensor based on SnO_2/rGO were 11 and 6 min while respectively, whereas those of sensor based on SnO_2 were 13 and 9 min respectively. In addition, the resistance of SnO_2/rGO was higher than that of SnO_2 when exposed to air. A potential barrier exists at the interface between the n-type SnO_2 nanoparticle and p-type rGO, and depletion layers coexist in this p–n heterojunction. The potential barrier and depletion layers resulting from p–n junction modulate the resistance of SnO_2/rGO to show higher resistance than SnO_2 in air [34]. SnO_2 is a classical n-type semiconductor that increases resistance exposed to oxidant gas from air. The increased resistance of SnO_2/rGO in NO_2 indicated that the composite also exhibited n-type semiconductor behavior. In our case, the huge amount of SnO_2 provided a short path for carrier between discrete rGO sheets and dominated its n-type semiconductor behavior.

The relationship between response and NO_2 concentration for the sensor at operating temperature of 75 °C was displayed in Fig. 6, in which the logarithmic values of response are plotted as a function of NO_2 concentration. It was shown that the response increased with the NO_2 concentration in the range of 50 ppb to 2 ppm. The limit of detection was 50 ppb and the response of the sensor to 50 ppb NO_2 was 2.9. The good reproducibility of the sensor to 1 ppm NO_2 is shown in Fig. 7. During the five continuous

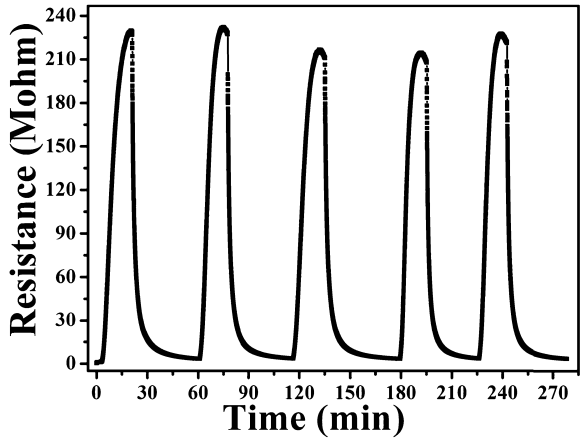

Fig. 7. The five periods of response transient of SnO_2/rGO to 1 ppm NO_2 at 75 °C.

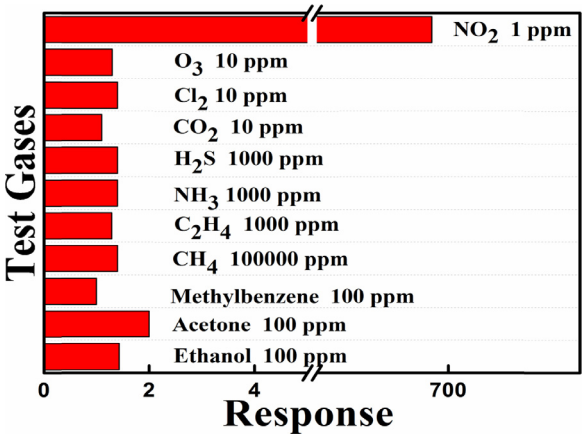

Fig. 8. The response of sensor based on SnO_2/rGO to various gases at 75 °C.

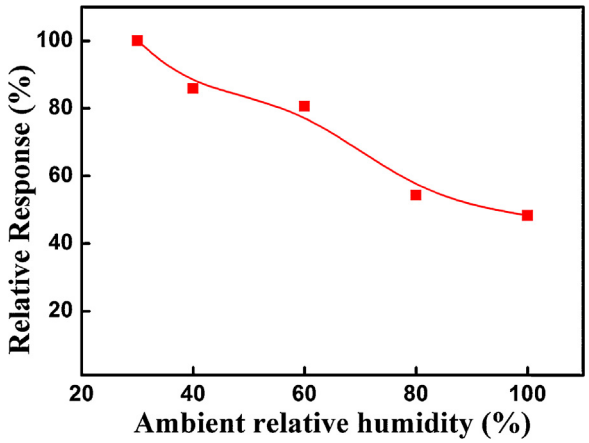

Fig. 9. Effect of ambient relative humidity on the response of sensor based SnO_2/rGO (1.4%) exposed to NO_2.

response/recovery cycles, the sensor exhibited approximately the same response value and response/recovery time.

The selectivity of the sensor was also studied, and the results shown in Fig. 8 illustrate the cross-responses of the sensor towards various tested gases, nmely H_2S, NH_3, Cl_2, O_3, methane, ethylene, toluene, acetone and ethanol. All the gases were tested at 75 °C with a much higher concentration (at least 10-fold) against NO_2. The responses of the sensor to various testing gases were lower than 2, while the response to NO_2 was ~700, which indicated the good selectivity to NO_2. The effect of environmental humidity on the response of sensor based SnO_2/rGO (1.4%) exposed to NO_2 has been studied, and the results are shown in Fig. 9. The sensor response decreased with increase in environmental humidity, and the response decreased to 50% when humidity was 100%.

Comparison of the NO_2 sensing performances of the sensors based on SnO_2/rGO or SnO_2/graphene is summarized in Table 1.

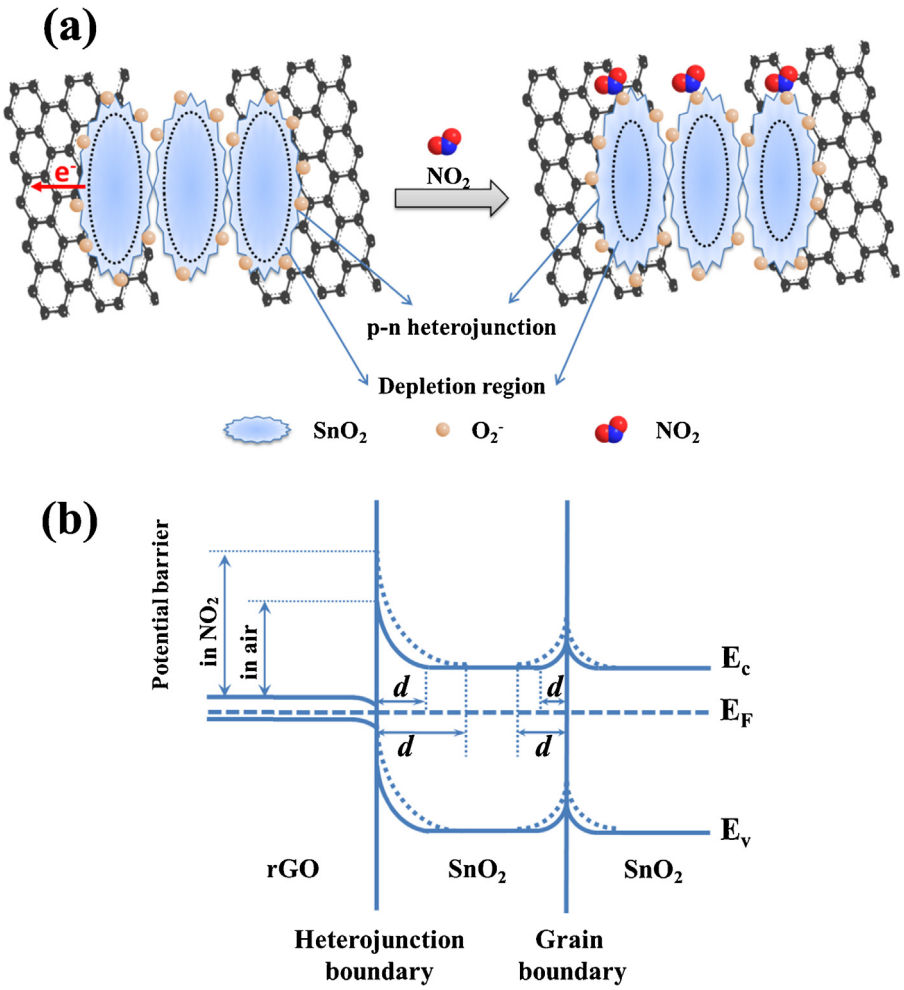

Fig. 10. Schematic illustration of the sensing mechanism of the NO_2 sensor based on SnO_2/rGO (a), model of a potential barrier to electronic conduction at heterojunction boundary and grain boundary (b).

Table 1
The sensing performance comparison of different SnO_2/graphene composites towards NO_2.

Sensing materials	Synthesis method	Optimum operating temperature (°C)	Sensing performance		Detection limit	Reference
			NO_2 concentration (ppm)	Response (R_g/R_a or R_a/R_g)		
SnO_2/rGO	Hydrothermal treatment	50	5	3.31	0.5 ppm	[25]
SnO_2/rGO	Hydrothermal treatment	45	100	1.083	14 ppm	[26]
SnO_2/rGO	Electrospinning	200	1	≈15	1 ppm	[34]
SnO_2/rGO	Thermal evaporation with CVD	150	0.1	≈11	10 ppb	[35]
SnO_2/rGO	Solvothermal treatment	Room temperature	10	$-4\%(\Delta R/R_a)$	10 ppm	[36]
SnO_2/rGO	Hydrothermal treatment	75	1	696	50 ppb	Present work

Compared with previous results in literatures [25,26,34–36], our sensor has improved detection limit to tens ppb level at a relatively low temperature and has a wider detection range, so it can be used as a promising trace NO_2 sensors with low power consumption. Although some SnO_2/rGO composites [25,26] were also synthesized by hydrothermal treatment, there are significant differences in the percentage and size/morphology of SnO_2 crystals in composites, which maybe have effect on the sensing performance.

As literatures reported [11,19,25,26,34,36,38], improved response of MOs-graphene-based sensor were always explained by two factors: (1) enhancement of the surface accessibility of SnO_2–rGO and (2) effective electronic interaction between SnO_2 nanocrystals and the rGO sheets. Since the operation of gas sensors involves adsorption/desorption processes and reactions at the interface, the surface accessibility of sensing material is crucial to achieve high response [37]. The surface areas of the SnO_2 and SnO_2/rGO samples were determined by BET. The BET results demonstrate that the variation of the surface area with the absence and presence of rGO is negligible (23.5 $m^2\,g^{-1}$ for SnO_2, and 20.7 $m^2\,g^{-1}$ for SnO_2/rGO), and the even smaller surface area of SnO_2/rGO cannot contribute to positive effects on sensing performance. Thus, in this work, the modulations of material resistance play a major role in the sensing mechanism of SnO_2/rGO. The p–n heterojunction formed between the n-type SnO_2 and the p-type rGO displays significant effects on the resistance modulation of SnO_2/rGO [3,19,25,34,36,38]. In our case, SnO_2 was major content and covered a considerable part of the rGO surface and rGO had a discrete configuration. Thus main conduction would occur along continuous SnO_2, rather than along discrete rGO. SnO_2 is considered to be involved in the receptor function while the rGO mainly provides the electronic conduction path. The percentage of O element in our rGO sample can be calculated by XPS results, which is about 22%. The literatures reported the calculated work function and band gap of rGO with ~20% O content are about 5.4 eV [39] and 0.914 eV [40]. The work function of such rGO was higher than that of SnO_2 (4.8 eV), and hence in these p–n heterojunctions the discrete rGO as an electron-absorption body will receive electrons from adjacent SnO_2 resulting in modulation of the resistance of the composites. As shown as in Fig. 9–10, two different potential barriers and depletion layers coexist in SnO_2/rGO heterostructures. One is on the interface between SnO_2 nanograins and the other is at the interface between rGO and SnO_2. The two potential barriers will be changed by adsorption or desorption of gas molecules, resulting in additional modulation of the total resistance of the sensor. In the air, oxygen molecules are adsorbed on the surfaces of the SnO_2/rGO and ionized to O_2^-, O^- or O^{2-} by capturing free electrons from the SnO_2/rGO, which directly influences the resistance of the sensor. When exposed to NO_2, the adsorbed oxygen species interact with NO_2, causing the extraction of electrons to be extracted from SnO_2 and widening both depletion layers. Moreover, the monocrystalline nature of SnO_2 benefits electronic transmission and thin thickness of discoid SnO_2 facilitates the depletion of its surface by the adsorbed NO_2 which in turn strongly modifies the heterojunction layer, and therefore alters the whole resistance of the heterostructured sensor. Additionally, the interaction between SnO_2 and rGO may influence the redox and electronic properties of SnO_2 [41,42], that leads to more active sites for the adsorption and reaction of NO_2 molecules. In summary, the formation of p–n heterojunction and the morphology of SnO_2 nanograins contribute to tens ppb level of detection limit to NO_2.

4. Conclusions

In summary, novel discoid crystals of rutile SnO_2 modified by rGO nanosheets have been successfully synthesized using a facile one-step hydrothermal method. The as-synthesized SnO_2/rGO composites exhibited the morphology of the compact monodisperse SnO_2 discoid particles with the rGO flaky structure among them. The characterization results demonstrated that the rGO existed in composites and was successfully reduced from GO. The gas properties of this discoid SnO_2/rGO were measured and the results indicated that it showed high sensing performance to NO_2 at a low operating temperature with enhanced response, relatively short response and recovery time, good reproducibility and excellent selectivity, especially in detection limit as low as 50 ppb. The improved response was attributed to the modification of potential barrier at the SnO_2–rGO interface.

Acknowledgments

This work was supported by the National Natural Science Foundation of China (61134010, 61304242, 61327804, 61377058 and 61374218), Program for Chang Jiang Scholars and Innovative Research Team in University (No.IRT13018), National High-Tech Research and Development Program of China (863 Program, No. 2013AA030902 and 2014AA06A505), China Postdoctoral Science Foundation (No.2013M530979), Science and Technology Development Program of Jilin Province (No.20150520091JH).

References

[1] J.-P. Tessonnier, D. Rosenthal, T.W. Hansen, C. Hess, M.E. Schuster, R. Blume, F. Girgsdies, N. Pfänder, O. Timpe, D.S. Su, R. Schlögl, Analysis of the structure and chemical properties of some commercial carbon nanostructures, Carbon 47 (2009) 1779–1798.
[2] C. Baratto, G. Sberveglieri, A. Onischuk, B. Caruso, S. di Stasio, Low temperature selective NO_2 sensors by nanostructured fibres of ZnO, Sens. Actuators B: Chem. 100 (2004) 261–265.
[3] C. Marichy, P.A. Russo, M. Latino, J.-P. Tessonnier, M.-G. Willinger, N. Donato, G. Neri, N. Pinna, Tin dioxide-carbon heterostructures applied to gas sensing: structure-dependent properties and general sensing mechanism, J. Phys. Chem. C 117 (2013) 19729–19739.
[4] J. Zhao, W. Wang, Y. Liu, J. Ma, X. Li, Y. Du, G. Lu, Ordered mesoporous Pd/SnO_2 synthesized by a nanocasting route for high hydrogen sensing performance, Sens. Actuators B: Chem. 160 (2011) 604–608.
[5] P. Sun, L. You, Y. Sun, N. Chen, X. Li, H. Sun, J. Ma, G. Lu, Novel Zn-doped SnO_2 hierarchical architectures: synthesis, characterization, and gas sensing properties, CrystEngComm 14 (2012) 1701–1708.
[6] S. Gubbala, V. Chakrapani, V. Kumar, M.K. Sunkara, Band-edge engineered hybrid structures for dye-sensitized solar cells based on SnO_2 nanowires, Adv. Funct. Mater. 18 (2008) 2411–2418.

[7] M.A. Hossain, J.R. Jennings, Z.Y. Koh, Q. Wang, Carrier generation and collection in CdS/CdSe-sensitized SnO_2 solar cells exhibiting unprecedented photocurrent densities, ACS Nano 5 (2011) 3172–3181.
[8] Y.-S. Lin, J.-G. Duh, M.-H. Hung, Shell-by-shell synthesis and applications of carbon-coated SnO_2 hollow nanospheres in lithium-ion battery, J. Phys. Chem. C 114 (2010) 13136–13141.
[9] J. Ye, H. Zhang, R. Yang, X. Li, L. Qi, Morphology-controlled synthesis of SnO_2 nanotubes by using 1D silica mesostructures as sacrificial templates and their applications in lithium-ion batteries, Small 6 (2010) 296–306.
[10] E.N. Dattoli, Q. Wan, W. Guo, Y. Chen, X. Pan, W. Lu, Fully transparent thin-film transistor devices based on SnO_2 nanowires, Nano Lett. 7 (2007) 2463–2469.
[11] I.-S. Kang, H.-M. So, G.-S. Bang, J.-H. Kwak, J.-O. Lee, C.W. Ahn, Recovery improvement of graphene-based gas sensors functionalized with nanoscale heterojunctions, Appl. Phys. Lett. 101 (2012) 123504.
[12] C. Wang, X. Cheng, X. Zhou, P. Sun, X. Hu, K. Shimanoe, G. Lu, N. Yamazoe, Hierarchical alpha-Fe_2O_3/NiO composites with a hollow structure for a gas sensor, ACS Appl. Mat. Interfaces 6 (2014) 12031–12037.
[13] L.T.T. Tuyen, K. Potje-Kamloth, H.D. Liess, Electrical properties of doped polypyrrole/silicon heterojunction diodes and their response to NO_x gas, Thin Solid Films 292 (1997) 293–298.
[14] J. Gong, Y. Li, Z. Hu, Z. Zhou, Y. Deng, Ultrasensitive NH_3 gas sensor from polyaniline nanograin enchased TiO_2 fibers, J. Phys. Chem. C 114 (2010) 9970–9974.
[15] X. Xue, L. Xing, Y. Chen, S. Shi, Y. Wang, T. Wang, Synthesis and H_2S sensing properties of CuO–SnO_2 core/shell PN-junction nanorods, J. Phys. Chem. C 112 (2008) 12157–12160.
[16] C.N.R. Rao, A.K. Sood, K.S. Subrahmanyam, A. Govindaraj, Graphene: the new two-dimensional nanomaterial, Angew. Chem. Int. Ed. 48 (2009) 7752–7777.
[17] G. Lu, L.E. Ocola, J. Chen, Reduced graphene oxide for room-temperature gas sensors, Nanotechnology 20 (2009) 445502.
[18] X. An, J.C. Yu, Y. Wang, Y. Hu, X. Yu, G. Zhang, WO_3 nanorods/graphene nanocomposites for high-efficiency visible-light-driven photocatalysis and NO_2 gas sensing, J. Mater. Chem. 22 (2012) 8525–8531.
[19] G. Neri, S.G. Leonardi, M. Latino, N. Donato, S. Baek, D.E. Conte, P.A. Russo, N. Pinna, Sensing behavior of SnO_2/reduced graphene oxide nanocomposites toward NO_2, Sens. Actuators B: Chem. 179 (2013) 61–68.
[20] S. Shubhda, J. Kiran, V.N. Singh, S. Sukhvir, N. Vijayan, D. Nita, G. Govind, T.D. Senguttuvan, Faster response of NO_2 sensing in graphene–WO_3 nanocomposites, Nanotechnology 23 (2012) 205501.
[21] P.A. Russo, N. Donato, S.G. Leonardi, S. Baek, D.E. Conte, G. Neri, N. Pinna, Room-temperature hydrogen sensing with heteronanostructures based on reduced graphene oxide and tin oxide, Angew. Chem. Int. Ed. 51 (2012) 11053–11057.
[22] Z. Zhang, R. Zou, G. Song, L. Yu, Z. Chen, J. Hu, Highly aligned SnO_2 nanorods on graphene sheets for gas sensors, J. Mater. Chem. 21 (2011) 17360–17365.
[23] S.-J. Choi, B.-H. Jang, S.-J. Lee, B.K. Min, A. Rothschild, I.-D. Kim, Selective detection of acetone and hydrogen sulfide for the diagnosis of diabetes and halitosis using SnO_2 nanofibers functionalized with reduced graphene oxide nanosheets, ACS Appl. Mat. Interfaces 6 (2014) 2588–2597.
[24] Q. Lin, Y. Li, M. Yang, Tin oxide/graphene composite fabricated via a hydrothermal method for gas sensors working at room temperature, Sens. Actuators B: Chem. 173 (2012) 139–147.
[25] H. Zhang, J. Feng, T. Fei, S. Liu, T. Zhang, SnO_2 nanoparticles-reduced graphene oxide nanocomposites for NO_2 sensing at low operating temperature, Sens. Actuators B: Chem. 190 (2014) 472–478.
[26] L. Li, S. He, M. Liu, C. Zhang, W. Chen, Three-dimensional mesoporous graphene aerogel-supported SnO_2 nanocrystals for high-performance NO_2 gas sensing at low temperature, Anal. Chem. 87 (2015) 1638–1645.
[27] Y. Gao, Y. Li, L. Zhang, H. Huang, J. Hu, S.M. Shah, X. Su, Adsorption and removal of tetracycline antibiotics from aqueous solution by graphene oxide, J. Colloid Interface Sci. 368 (2012) 540–546.
[28] Z. Wang, Y. Xiao, X. Cui, P. Cheng, B. Wang, Y. Gao, X. Li, T. Yang, T. Zhang, G. Lu, Humidity-sensing properties of urchin like CuO nanostructures modified by reduced graphene oxide, ACS Appl. Mat. Interfaces 6 (2014) 3888–3895.
[29] P. Sun, W. Zhao, Y. Cao, Y. Guan, Y. Sun, G. Lu, Porous SnO_2 hierarchical nanosheets: hydrothermal preparation, growth mechanism, and gas sensing properties, Cryst. Eng. Comm. 13 (2011) 3718–3724.
[30] L. Huang, Y. Liu, L.-C. Ji, Y.-Q. Xie, T. Wang, W.-Z. Shi, Pulsed laser assisted reduction of graphene oxide, Carbon 49 (2011) 2431–2436.
[31] X. Li, H. Wang, J.T. Robinson, H. Sanchez, G. Diankov, H. Dai, Simultaneous nitrogen doping and reduction of graphene oxide, J. Am. Chem. Soc. 131 (2009) 15939–15944.
[32] S.F. Bamsaoud, S.B. Rane, R.N. Karekar, R.C. Aiyer, Nano particulate SnO_2 based resistive films as a hydrogen and acetone vapour sensor, Sens. Actuators B 153 (2011) 382–391.
[33] C. Feng, X. Li, J. Ma, Y. Sun, C. Wang, P. Sun, J. Zheng, G. Lu, Facile synthesis and gas sensing properties of In2O3-WO3 heterojunction nanofibers, Sens. Actuators B: Chem. 209 (2015) 622–629.
[34] J.-H. Lee, A. Katoch, S.-W. Choi, J.-H. Kim, H.W. Kim, S.S. Kim, Extraordinary improvement of gas-sensing performances in SnO_2 nanofibers due to creation of local p–n heterojunctions by loading reduced graphene oxide nanosheets, ACS Appl. Mat. Interfaces 7 (2015) 3101–3109, 11009.
[35] Q. Vu Van, D. Nguyen Van, T. Ngo Sy, H. Nguyen Duc, D. Nguyen Van, H. Nguyen Van, Outstanding gas-sensing performance of graphene/SnO_2 nanowire Schottky junctions, Appl. Phys. Lett. 105 (2014) 013107.
[36] X. Liu, J. Cui, J. Sun, X. Zhang, 3D graphene aerogel-supported SnO_2 nanoparticles for efficient detection of NO_2, RSC Adv. 4 (2014) 22601–22605.
[37] S. Deng, V. Tjoa, H.M. Fan, H.R. Tan, D.C. Sayle, M. Olivo, S. Mhaisalkar, J. Wei, C.H. Sow, Reduced graphene oxide conjugated Cu_2O nanowire mesocrystals for high-performance NO_2 gas sensor, J. Am. Chem. Soc. 134 (2012) 4905–4917.
[38] S. Mao, S. Cui, G. Lu, K. Yu, Z. Wen, J. Chen, Tuning gas-sensing properties of reduced graphene oxide using tin oxide nanocrystals, J. Mater. Chem. 22 (2012) 11009–11013.
[39] P.V. Kumar, M. Bernardi, J.C. Grossman, The impact of functionalization on the stability, work function, and photoluminescence of reduced graphene oxide, ACS Nano 7 (2013) 1638–1645.
[40] H. Huang, Z. Li, J. She, W. Wang, Oxygen density dependent band gap of reduced graphene oxide, J. Appl. Phys. 111 (2012) 054317.
[41] T. Ressler, A. Walter, J. Scholz, J.P. Tessonnier, D.S. Su, Structure and properties of a Mo oxide catalyst supported on hollow carbon nanofibers in selective propene oxidation, J. Catal. 271 (2010) 305–314.
[42] K. Mette, A. Bergmann, J.-P. Tessonnier, M. Hävecker, L. Yao, T. Ressler, R. Schlögl, P. Strasser, M. Behrens, Nanostructured manganese oxide supported on carbon nanotubes for electrocatalytic water splitting, Chem. Cat. Chem. 4 (2012) 851–862.

Biographies

Yan Xiao is currently working toward the MS degree in the Electronics Science and Engineering department, Jilin University. Her research interests include the synthesis of graphene functionalized metal oxide semiconductor materials and their applications in gas sensors.

Qiuyue Yang received her BS degree from Electronics Science and Engineering Department, Jilin University, China in 2013. Presently, she is a graduate student, majored in microelectronics and solid state electronics.

Zhenyu Wang received his BS degree from the Electronics Science and Engineering Department, Jilin University, China in 2010. He received his Ph.D. degree, majoring in microelectronics and solid state electronics, from the Electronics Science and Engineering Department, Jilin University, China in 2015. Presently, he is a lecture in School of Ocean Science & Technology, Dalian University of Technology.

Rui Zhang is a senior student in the Electronics Science and Engineering department, Jilin University.

Yuan Gao received her Ph.D. degree from the Department of Analytical Chemistry at Jilin University in 2012. She is currently a lecturer in Jilin University, China. Her current research is focused on the preparation and application of graphene oxide and semiconductor oxide, especially in gas sensosr and biosensors.

Peng Sun received his Ph.D. degree from the Electronics Science and Engineering department, Jilin University, China in 2014. Now, he is engaged in the synthesis and characterization of the semiconducting functional materials and gas sensors.

Yanfeng Sun obtained his Ph.D. from Jilin University of China in 2007. Presently, he is working as associate professor in Electronics Science and Engineering department of Jilin University. His current research interests are nanoscience and gas sensors.

Geyu Lu received the BS degree in electronic sciences in 1985 and the MS degree in 1988 from Jilin University in China and the Dr Eng degree in 1998 from Kyushu University in Japan. Now he is a professor of Jilin University, China. Now, he is interested in the development of functional materials and chemical sensors.